

Theoretical modelling and experimental study of spacer-filled direct contact membrane distillation: effect of membrane thermal conductivity model selection

Quoc Linh Ve^{a,*}, Ravi Koirala^a, Mohammed Bawahab^a, Hosam Faqeha^a, Minh Cuong Do^b, Quang Lich Nguyen^c, Abhijit Date^a, Aliakbar Akbarzadeh^a

^aMechanical and Automotive Engineering, School of Engineering, RMIT University, Bundoora, Victoria 3083, Australia, Tel. +61-420251709; emails: s3633369@student.rmit.edu.au/vequoclinh@huaf.edu.vn/vqlinh@hueuni.edu.vn (Q. Linh Ve), s3685308@student.rmit.edu.au (R. Koirala), s3423937@student.rmit.edu.au (M. Bawahab), s3695038@student.rmit.edu.au (H. Faqeha), abhijit.date@rmit.edu.au (A. Date), aliakbar.akbarzadeh@rmit.edu.au (A. Akbarzadeh)

^bFaculty of Engineering and Food Technology, University of Agriculture and Forestry, Hue University, Thua Thien Hue, 530000, Vietnam, email: dominhcuong@huaf.edu.vn

^cSchool of Engineering and Technology, Hue University, Thua Thien Hue, 530000, Vietnam, email: nguyenquanglich@hueuni.edu.vn

Received 19 March 2020; Accepted 7 December 2020

ABSTRACT

This research aimed to examine the effect of the thermal conductivity model of hydrophobic membranes on performance modelling of direct contact membrane distillation systems. The parallel, series, and two types of Maxwell models were studied. Simultaneously, an iterative numerical model was developed to choose the most appropriate model by analysing the mass flux (J_m) and the heat transfer rate (\dot{Q}_p). Comparison with the experimental results, showing that Maxwell Type II was the most appropriate for modelling the thermal conductivity of the membrane. Also, based on the chosen model of membrane thermal conductivity, the direct contact membrane distillation performance (the global heat transfer coefficient, temperature polarization coefficient, energy efficiency, and gain output ratio) was studied. It was found that the membrane thermal conductivity model with a higher value of membrane thermal conductivity (k_m) resulted in an underestimation of the predicted mass flux, temperature polarization coefficient, and energy efficiency. In contrast, the total heat transfer coefficient and predicted heat rate were overestimated. The gain output ratio values seemed not to be affected by this choice with only 8% deviation among the four models.

Keywords: Direct contact membrane distillation; Membrane thermal conductivity; Theoretical modelling; Mass flux; Heat transfer rate

1. Introduction

Membrane distillation is a separation process that allows only vapour molecule transport through porous hydrophobic membranes. This process is complicated because both the heat and mass transfer occur at the same time. The calculation of thermal conductivity of the membrane is a combination of thermal conductivity of polymer, water

vapour, and air. Therefore, accurate determination of the thermal conductivity value of the membrane for modelling is not simple. There are two conventional models used in membrane distillation literature for predicting the thermal conductivity: the parallel model (isostrain, Eq. (14)) [1–6] and the series model (isostress, Eq. (15)) [2,6,7].

For the parallel model, it is assumed that the polymer layers of the membrane and the heat flux are aligned

* Corresponding author.

in the same direction, whereas the heat flux is assumed to be perpendicular to the gas/polymer layers, which are equally spaced in the series model. Therefore, the calculation of membrane thermal conductivity using these models is limiting as mentioned above. Phattaranawik et al. [2] performed an estimation of thermal conductivity of polyvinylidene fluoride (PVDF) and polytetrafluoroethylene (PTFE) membrane by using the parallel, series, and flux law model. The calculated results from the three models were compared with reported values in other studies and acquired the most appropriate model. In this study, the series model had the best agreement between calculated and reported values, whereas the most inaccurate model belonged to the parallel model.

García-Payo and Izquierdo-Gil [7] performed an extensive investigation of thermal conductivity of different membranes, including 2 PTFE, 2 PVDF, and 2 PTFE membranes with supported layers by using nine different models. Then, the predicted values were compared to experimental data. As concluded in this study, the thermal conductivity was largely overestimated if the parallel model was used, whereas the series model slightly underestimated it. The Maxwell Type I model was proposed for the best fit model for all tested membranes when the membrane's porosity was higher than 60%. In Maxwell's models, the polymer particles in the membrane are assumed to be distributed randomly and do not have any mutual interaction in a homogeneous medium (air) [7].

Plamenov [6] also estimated the thermal conductivity of seven commercially available membranes by using three models: parallel, series, and Maxwell Type I model. Similarly, the Maxwell Type I model was proposed for the prediction of thermal conductivity of the membrane instead of the series or parallel model. Gonzo [8] developed correlations to calculate the effective thermal conductivity with respect to three main groups of porous materials: Type A (low-density porous materials, porosity higher than 90%), Type B (medium-density materials, porosity in the range 15%–85%), Type C (high-density materials, porosity up to 10%). The study pointed out that Maxwell's correlation was the best thermal conductivity model for low-density and medium-density porous materials.

In most studies with regard to water productivity and energy efficiency improvement in direct contact membrane distillation (DCMD) module, different commercial hydrophobic membranes were investigated [2,9–19]. All parameters of the membrane could be provided by manufacturers or tested by experimental methodologies with the exception of thermal conductivity. Therefore, the DCMD outputs reported in existing studies could be different depending on which model of membrane thermal conductivity was employed. Indeed, in comparison with other membrane distillation process, DCMD has lower thermal efficiency [20,21]. There are some solutions to increase the energy efficiency of the DCMD system, for example increasing the feed solution temperature [9,20,22–25], increasing the flow rate of feed solution [9,23–27] or coupling the DCMD system with heat recovery devices through low-grade heat sources [9,25,28–31]. Furthermore, using lower thermal conductivity membranes could result in higher permeate flux and higher energy efficiency. Al-Obaidani et al. [9]

examined the effect of membrane thermal conductivity on permeate flux and thermal efficiency in a hollow fiber DCMD module. Based on the experimental input parameters from an existing membrane, the simulated results pointed out that permeate flux and thermal efficiency were lower for the membrane with higher thermal conductivity. A similar trend was also provided by Loussif and Orfi [10] with a 14.52% decrease in permeate flux when the thermal conductivity of the membrane increased from 0.05 to 0.35 W m⁻¹ K⁻¹. Vanneste et al. [11] tested the permeate flux and thermal efficiency in the DCMD module with 17 hydrophobic membranes made from different materials like polypropylene (PP), ethylene chlorotrifluoroethylene, polyethylene. The experimental results suggested that the membrane with smaller thermal conductivity could result in higher permeate flux and thermal efficiency.

From the literature, the membrane thermal conductivity was a key factor affecting the permeate flux and energy efficiency in the DCMD process/system. The choice of membrane thermal conductivity model thus plays a vital role in obtaining the best agreement between theoretical and experimental results. Using different models of membrane thermal conductivity can result in the value varying by a factor of 2 or more. Due to this uncertainty, DCMD performance was often overestimated or underestimated in comparison to experimental data. However, the prior studies lacked methodologies for selecting the thermal conductivity model. Therefore, this study aims to propose a more accurate methodology for selecting the appropriate theoretical model for membrane thermal conductivity. This is based on experimental data analysing the mass flux and heat balance in the DCMD process.

2. Theory

2.1. Flow mechanisms

The working mechanisms of cross-flow membranes are classified into Knudsen diffusion, molecular diffusion, and Poiseuille flow. However, in the DCMD module, viscous flow is neglected because both the feed and permeate solution directly contact the surface of the membrane under atmospheric pressure (10⁵ Pa) [2,5,32,33]. Therefore, for mass transfer through the hydrophobic membrane, only the Knudsen flow model, the ordinary molecular diffusion model, and the Knudsen-molecular combination model are proposed [5,32]. Furthermore, Schofield et al. [1,12,34,35] mentioned that the flux of water across the membrane is much larger than airflow thus, viscous flow can be negligible if the solutions are not degassed.

For a given membrane parameter and experimental condition, to determine the mechanism of mass transfer through the porous membrane, the Knudsen number (Kn) is used:

$$\text{Kn} = \frac{\lambda_w}{d_p} \quad (1)$$

where λ_w is the mean free path of water molecules can be estimated [3,21,36]:

$$\lambda_w = \frac{k_B T_m}{\sqrt{2\pi P_m d_e^2}} \quad (2)$$

To identify the flow mechanism inside the membrane pores, the Knudsen number (Kn) can be used for classification. If $Kn < 0.01$, the dominant mechanism is molecular diffusion, if $0.01 < Kn < 1$, the primary mechanism is combined Knudsen-molecular diffusion and if Kn is larger than 1, the Knudsen mechanism dominates.

Membrane tortuosity is determined by using the calculation proposed by [3]:

$$\tau = \frac{1}{\varepsilon} \quad (3)$$

2.2. Mass transfer in direct contact membrane distillation

In the DCMD process, due to the temperature difference, which results in pressure difference, the water molecules transfer from the higher pressure side (feed) to the lower pressure side (permeate). Therefore, there is a linear relationship between the experimental mass flux and the vapour pressure difference across the membrane [1,3,21,32,33]:

$$J_w = C_m (p_{v,swf} - p_{v,swp}) \quad (4)$$

where $p_{v,swf}$ and $p_{v,swp}$ are the partial pressures of water vapour estimated at $T_{m,f}$ and $T_{m,p}$ by using Sharqawy's equation [37]. This proposed equation was applied in the range of temperature (0°C–180°C) and the range of solution salinity (0–160 g/kg) for natural seawater:

$$p_{v,sw} = p_{v,w} \times \exp(-4.58180 \times 10^{-4} S - 2.04430 \times 10^{-6} S^2) \quad (5)$$

where $p_{v,w} = \exp(a_1/T_{m,f(p)} + a_2 + a_3 T_{m,f(p)} + a_4 T_{m,f(p)}^2 + a_5 T_{m,f(p)}^3 + a_6 \ln(T_{m,f(p)}))$, $a_1 = -5,800$; $a_2 = 1.3915$; $a_3 = -4.8640 \times 10^{-2}$; $a_4 = 4.1765 \times 10^{-5}$; $a_5 = -1.4452 \times 10^{-8}$; $a_6 = 6.5460$.

The membrane distillation coefficient C_m can be estimated by using the following correlations [3,21]:

C_m for Knudsen flow mechanisms:

$$C_m^K = \frac{2}{3RT} \frac{\varepsilon r}{\tau \delta} \left(\frac{8RT}{\pi M} \right)^{1/2} \quad (6)$$

C_m for molecular diffusion:

$$C_m^D = \frac{\varepsilon}{\tau \delta} \frac{PD}{P_a} \frac{M}{RT} \quad (7)$$

C_m for Knudsen-molecular diffusion mechanism:

$$C_m^C = \frac{1}{RT\delta} \left(\frac{3\tau}{2\varepsilon r} \left(\frac{\pi M}{8RT} \right)^{1/2} + \frac{p_a \tau}{\varepsilon PD} \right)^{-1} \quad (8)$$

For water/air, PD (Pa.m²/s) is estimated [21]:

$$PD = 1.895 \times 10^{-5} T_m^{2.072} \quad (9)$$

2.3. Heat transfer in DCMD

The heat transfer in DCMD can be divided into three regions as shown in Fig. 1: (1) heat transfer across liquid boundary layer due to convection in the feed side; (2) heat transfer across the hydrophobic membrane; (3) heat transfer across liquid boundary layer due to convection in the permeate side.

Across the liquid boundary layer at the feed and permeate side, the convective heat transfer rate can be written with Eqs. (10) and (11).

$$\dot{Q}_f = h_f \times A \times (T_f - T_{m,f}) \quad (10)$$

$$\dot{Q}_p = h_p \times A \times (T_{m,p} - T_p) \quad (11)$$

The rate of heat transfer through the membrane, \dot{Q}_m , is due to conduction heat loss through membrane matrix (\dot{Q}_c) and the latent heat transfer by vapour through the membrane pores (\dot{Q}_v) [21]:

$$\dot{Q}_m = \dot{Q}_c + \dot{Q}_v = \frac{k_m}{\delta} \times A \times (T_{m,f} - T_{m,p}) + J_w \times A \times \Delta H_{v,w} \quad (12)$$

where $\Delta H_{v,w}$ (kJ/kg) is vapour enthalpy of water evaluated at the mean membrane surface temperature T_m (K) using the following equation [3]:

$$\Delta H_{v,w} = 1.7535 \times T_m + 2,024.3 \quad (13)$$

where T_f and T_p are the bulk temperature at the feed and permeate side, respectively, which is mentioned in [38,39].

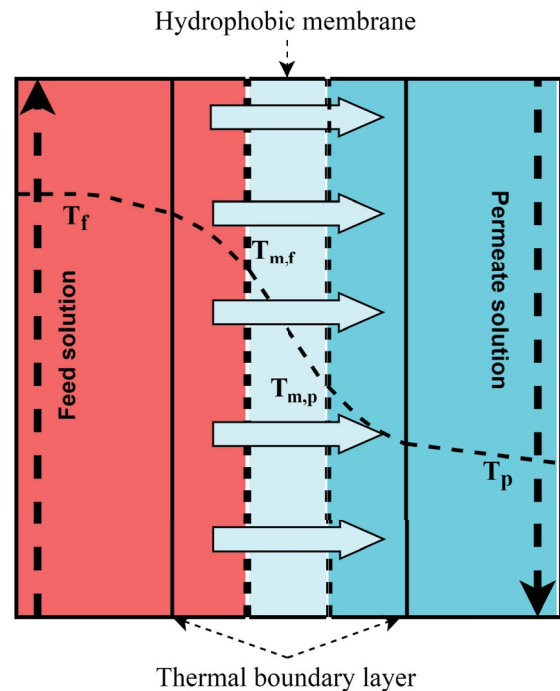


Fig. 1. Working principle of the DCMD process.

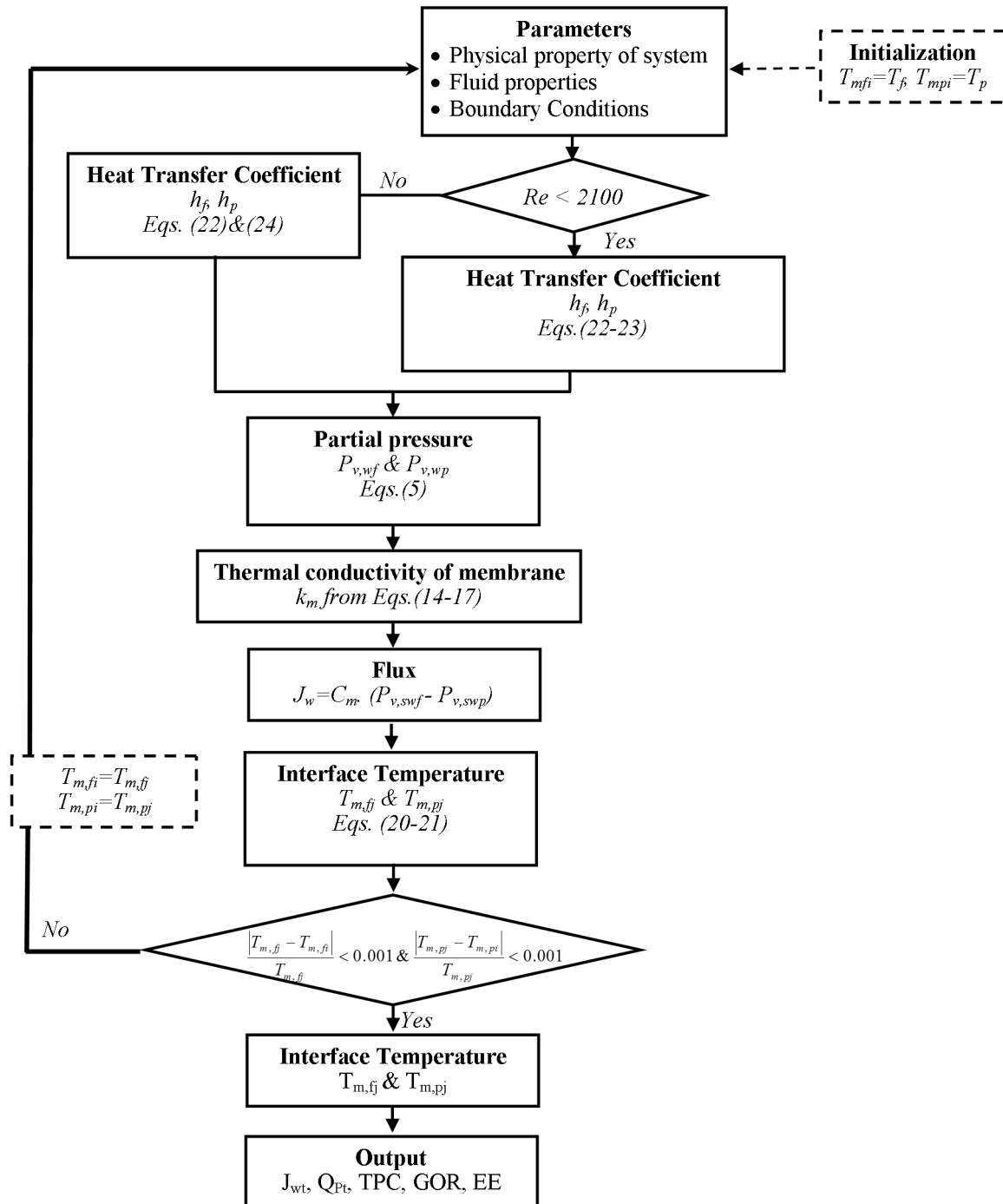


Fig. 2. Iterative numerical model.

For the thermal conductivity of the membrane, k_m , four models are suggested in Table 1 to predict k_m .

In these equations, k_p and k_g are the thermal conductivity of the membrane material and the gas phase inside the membrane pores, respectively. The thermal conductivities of water vapour and air are $0.020 \text{ W m}^{-1} \text{ K}^{-1}$ at 298 K and $0.022 \text{ W m}^{-1} \text{ K}^{-1}$ at 348 K for water vapour, and $0.026 \text{ W m}^{-1} \text{ K}^{-1}$ at 298 K, $0.028 \text{ W m}^{-1} \text{ K}^{-1}$ at 323 K and $0.030 \text{ W m}^{-1} \text{ K}^{-1}$ at 348 K for air [2,7]. Due to the small deviation between the

thermal conductivities of vapour and air, gases in the pore can be assumed as one component. The thermal conductivity of PTFE is estimated $0.25\text{--}0.27 \text{ W m}^{-1} \text{ K}^{-1}$ at 296 K, $0.28 \text{ W m}^{-1} \text{ K}^{-1}$ at 323 K and $0.29 \text{ W m}^{-1} \text{ K}^{-1}$ at 348 K [2,7,21]. Therefore, for this study, the values of $k_g = 0.027 \text{ W m}^{-1} \text{ K}^{-1}$ and $k_p = 0.27 \text{ W m}^{-1} \text{ K}^{-1}$ are assumed to calculate k_m . The porosity of the PTFE membrane is evaluated at 80% [16].

Assuming that the heat flow through each part must be equal the steady-state conditions:

Table 1
Theoretical models for predicting the thermal conductivity of the membrane

Model	Equation	No.	References
Parallel	$k_m = \varepsilon k_g + (1 - \varepsilon)k_p$	(14)	[3,5,7,33,40–45]
Series	$k_m = \left[\frac{\varepsilon}{k_g} + \frac{(1 - \varepsilon)}{k_p} \right]^{-1}$	(15)	[2,7,40]
Maxwell (Type I)	$k_m = \frac{k_g(1 + 2\beta\phi)}{1 - \beta\phi}$	(16)	[6,7]
Maxwell (Type II)	$k_m = \frac{k_g \left[1 + 2\beta\phi + (2\beta^3 - 0.1\beta)\phi^2 + 0.05\phi^3 \exp(4.5\beta) \right]}{1 - \beta\phi}$	(17)	[7,8]
	$\beta = (k_p - k_g)/(k_p + 2k_g)$		
	$\phi = 1 - \varepsilon$		

$$\dot{Q}_f = \dot{Q}_m = \dot{Q}_p \tag{18}$$

The global heat transfer coefficient can be derived [3]:

$$U = \left[\frac{1}{h_f} + \frac{1}{k_m / \delta + J_w \Delta H_{v,w} / (T_{m,f} - T_{m,p})} + \frac{1}{h_p} \right]^{-1} \tag{19}$$

For $T_{m,f}$ and $T_{m,p}$, it is not allowed to measure them by experiment. Therefore, the numerical model based on energy balance and Eqs. (10)–(12) needs to be developed with MATLAB (Fig. 2) to define the surface temperature at the feed-membrane and permeate-membrane side by using the two following Eqs. (20) and (21):

$$T_{m,f} = \frac{h_m \left(T_p + \frac{h_f}{h_p} T_f \right) + h_f T_f - J_w \Delta H_{v,w}}{h_m + h_f \left(1 + \frac{h_m}{h_p} \right)} \tag{20}$$

$$T_{m,p} = \frac{h_m \left(T_f + \frac{h_p}{h_f} T_p \right) + h_p T_p - J_w \Delta H_{v,w}}{h_m + h_p \left(1 + \frac{h_m}{h_f} \right)} \tag{21}$$

Heat transfer coefficients h_f , h_p can be estimated from dimensionless Nusselt numbers.

$$Nu_{f \text{ or } p} = \frac{h_{f \text{ or } p} \times d_h}{k_{f \text{ or } p}} \tag{22}$$

Nusselt number correlations under the effect of spacers were mentioned in aforementioned studies for laminar and turbulent regime flow [38,39,46].

For laminar regime flow:

$$Nu = 0.664 Re^{0.5} Pr^{0.33} \left(\frac{d_h}{L_m} \right)^{0.5} \tag{23}$$

For turbulent regime flow:

$$Nu = 0.023 \times \left(1 + 6 \left(\frac{d_h}{L} \right) \right) Re^{0.8} Pr^{1/3} \tag{24}$$

The Reynolds number (Re) and Prandtl number (Pr) can be determined straightforwardly through fluid properties using Sharqawy's correlation for seawater in both the feed and permeate side [37].

With the inlet and outlet temperature measurements in the feed and permeate side, the energy balance is given in counter-current flow:

$$\dot{Q}_p = \dot{Q}_m = \dot{Q}_f - Q_{\text{loss}} \tag{25}$$

In Eq. (25), heat produced by the feed (\dot{Q}_f) and heat absorbed by the permeate (\dot{Q}_p) were defined respectively by Eqs. (26)–(27) [38,39,41]:

$$\dot{Q}_f = \dot{m}_f C_{p,f} (T_{f,\text{in}} - T_{f,\text{out}}) \tag{26}$$

$$\dot{Q}_p = \dot{m}_p C_{p,p} (T_{p,\text{out}} - T_{p,\text{in}}) \tag{27}$$

The theoretical heat transfer rate was determined by using the log mean temperature difference approach via [47]:

$$\dot{Q}_{\text{pt}} = U \times A \times \Delta T_{\text{LMTD}} \tag{28}$$

where

$$\Delta T_{\text{LMTD}} = \frac{(T_{f,\text{in}} - T_{p,\text{out}}) - (T_{f,\text{out}} - T_{p,\text{in}})}{\ln \left[\frac{(T_{f,\text{in}} - T_{p,\text{out}})}{(T_{f,\text{out}} - T_{p,\text{in}})} \right]} \tag{29}$$

To find the most appropriate theoretical model for the thermal conductivity of the membrane, the theoretical mass flux (J_{wt}) and heat rate (\dot{Q}_t) are determined first. Then, in comparison with the experimental mass flux (J_w) and heat rate (\dot{Q}_p), the most appropriate model for the thermal conductivity of the membrane was selected with the least deviation of the theoretical results from the experimental results.

$$DEV = \frac{|\text{Experimental result} - \text{Theoretical result}|}{\text{Experimental result}} \times 100(\%) \quad (30)$$

For DCMD efficiency, the convective heat transfer through the liquid boundary layers is the limiting factor. Boundary layer resistance can be modelled by temperature polarization coefficient (TPC). Moreover, the reduction in the driving force (i.e., vapour pressure difference) resulting in the drop of freshwater production in DCMD can be reflected through the TPC. This coefficient is estimated as:

$$TPC = \frac{T_{m,f} - T_{m,p}}{T_f - T_p} \quad (31)$$

For spacer characteristics, all parameters such as filament diameter, mesh size, spacer thickness, porosity, as well as the hydraulic diameter for spacer-filled channels are mentioned in the previous study [38,39].

2.4. Energy efficiency and gain output ratio in DCMD

In most research, only the energy efficiency (EE) of membrane modules was introduced [28]. The EE is the ratio between the latent heat used for evaporation and the total heat transported through the membrane:

$$EE = \frac{J_w A \Delta H_{v,w}}{\dot{Q}_m} \quad (32)$$

The effective utilization of energy input to produce the permeate flux is estimated through the gain output ratio (GOR) value [28]. If the GOR value is higher, the performance of the DCMD module is better. In the DCMD process, the GOR is calculated as [28]:

$$GOR = \frac{J_w A \Delta H_{v,w}}{\dot{Q}_F} \quad (33)$$

3. Experimental approach

The lab-scale set-up with the DCMD unit used in this study is shown in Fig. 3. The membrane cell is composed of two transparent acrylic sheets. Each sheet had a flow channel 180 mm × 180 mm × 4 mm relating to the length, width, and depth of the DCMD channel, respectively. The hydrophobic membrane used was PTFE with PP supported layer (MSPTFEDT0221BX), manufactured by Membrane Solutions, LLC, (Shanghai, China). The nominal pore size and thickness of the membrane were 0.22 μm and (190–240 μm), respectively. To support the membrane, the stainless steel spacer mentioned in [38,39] was used on both sides of DCMD channels. In all experimental runs, to eliminate free convection, the DCMD module was placed vertically. The temperature of the feed solution (freshwater) was controlled by a hot water bath connected to a digital temperature controller. The freshwater at the permeate tank was cooled down to the required temperature by using a chiller connected to a plate heat exchanger and then pumped into the permeate channel. The flow was counter-current in the DCMD module with an equal volume flow rate (1 L/min). Two ultrasonic flow meters (UF25B, Cynergy3 Components Ltd., Wimborne, United Kingdom) placed before the inlet to the feed and permeate channel was used to measure the flow rates of both sides. The bulk temperatures of the liquid were measured at the inlet and outlet of both sides of the DCMD modules by thermocouples. A data logger (DT80 Datataker)

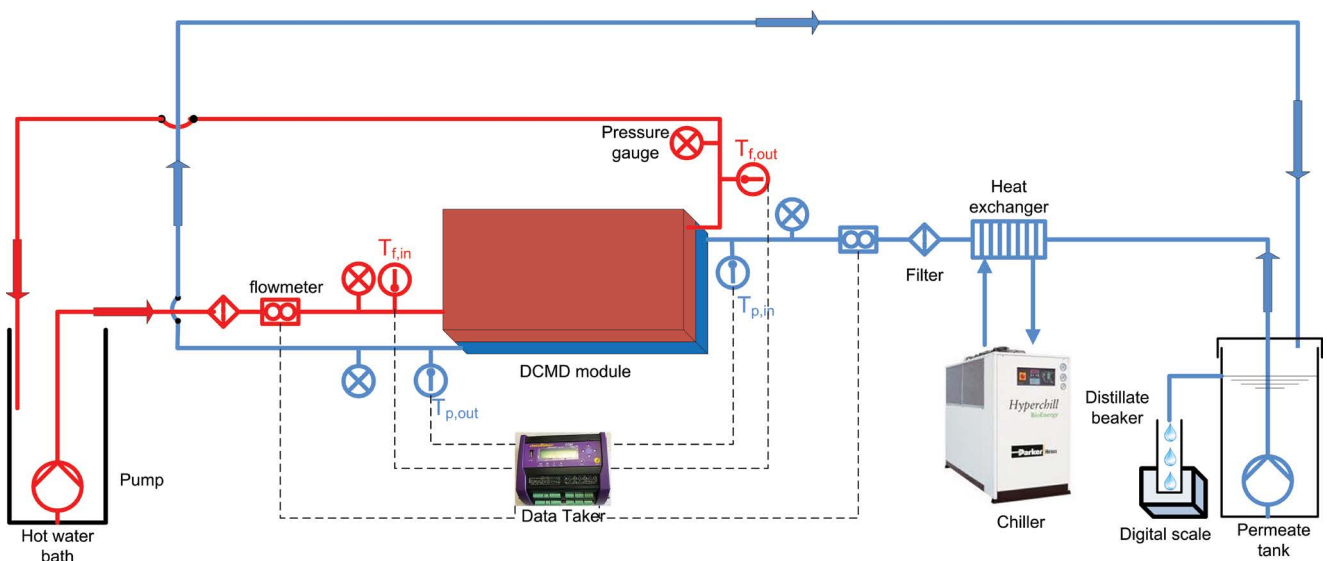


Fig. 3. DCMD setup for investigating heat and mass transfer.

was used for collecting measurements from thermocouples and flow meters over time. For pressure drop measurement, pressure gauges were positioned at the inlets and outlets of both sides. To ensure the accuracy of pressure gauge reading, manometers were also set up at the inlet and outlet of the feed side. The accumulated distillate water was determined over a time of 60 min using an electronic scale.

With fixed inlet temperatures on both sides, different experiments were conducted. The feed inlet temperature $T_{f,in}$ was varied 40°C to 60°C with 10°C increment, whereas the permeate inlet temperature $T_{p,in}$ was fixed at 20°C. Experimental repeatability was ensured with input parameters for modelling as shown in Table 2, and the random flow rate uncertainties at both sides were calculated to be 1.98%. In Table 2, the experimental repeatability (R1, R2, R3) was referred to with a reference number relating to feed inlet temperature (~50°C, ~60°C) and permeate inlet temperature (~20°C). The variation of all input parameters for simulation was lower than 5%. All uncertainties of measuring facilities are shown in Table 3.

At steady state, the accumulated distillate water over a period of time was used to calculate the experimental mass flux (J_w):

$$J_w (\text{kg m}^{-2} \text{ h}^{-1}) = \frac{\text{amount of accumulated distillate water (kg)}}{\text{membrane area (m}^2) \times \text{time (h)}} \tag{34}$$

3.1. Propagation of uncertainty of measurements

The Taylor series method (TSM) was used to calculate uncertainties. The uncertainties of experimental mass flux (J_w) and experimental heat rate (\dot{Q}_p) was determined based on the uncertainties of measuring devices in Table 3. The higher values of uncertainty are $\pm 0.0034 \text{ kg/m}^2\text{-h}$ for J_w and $\pm 52.62 \text{ W}$ for \dot{Q}_p .

4. Results and discussions

Based on the various models proposed in Table 1, the thermal conductivity of the PTFE membrane was calculated. The calculated values are shown in Table 4.

4.1. Permeability coefficient of the membrane (C_m)

The linear relationship between the experimental mass fluxes at various feed inlet temperatures and vapour

pressure differences ($p_{v,swf} - p_{v,swp}$) calculated at the membrane surface temperatures ($T_{m,f}$, $T_{m,p}$) were plotted and shown in Fig. 4. The membrane distillation coefficient, C_m' was determined as the slope of the straight line with reasonably high R-squared value ($R^2 > 0.998$). According to Fig. 4, the membrane permeability coefficient for pure water solution at the feed side was $3.89 \times 10^{-7} \text{ kg m}^{-2} \text{ s}^{-1} \text{ Pa}^{-1}$ under the effect of the stainless steel spacer (ST4). For theoretical modelling, the values of C_m were estimated from Eq. (8) at $3.72 \times 10^{-7} \text{ kg m}^{-2} \text{ s}^{-1} \text{ Pa}^{-1}$, $3.75 \times 10^{-7} \text{ kg m}^{-2} \text{ s}^{-1} \text{ Pa}^{-1}$, and $3.78 \times 10^{-7} \text{ kg m}^{-2} \text{ s}^{-1} \text{ Pa}^{-1}$ in the range of feed inlet temperature of 40°C, 50°C and 60°C, respectively. The maximum difference between the theoretical and semi-experimental C_m was only 4.3%. Therefore, in the range of investigated feed inlet temperature, C_m is assumed to be a constant value dependent upon the membrane characteristics and vapour properties.

4.2. Effect of membrane thermal conductivity model on predicted mass flux and heat transfer rate

The driving force resulting from the temperature difference between the feed-membrane and permeate-membrane interface allows vapour molecules to transport through the membrane pores. Using higher membrane thermal conductivity in modelling leads to a reduction

Table 3
Uncertainties of the measured data

T-type thermocouple	$\pm 0.5^\circ\text{C}$
Water flow meter	$\pm 3\%$ of the reading
Longitudinal dimensions	$\pm 0.01 \text{ mm}$
Electronic scale (weight)	$\pm 0.1 \text{ g}$
Time	$\pm 0.2 \text{ s}$

Table 4
Thermal conductivity of membrane for different models

Model	Calculated k_m (W/m-K)
Maxwell – Type I	0.0413
Maxwell – Type II	0.0426
Series (isostress)	0.0329
Parallel (isostrain)	0.0756

Table 2
Input parameters for repeatability in modelling

Repeatability	$T_{f,in}$ (°C)	$T_{f,out}$ (°C)	$T_{p,in}$ (°C)	$T_{p,out}$ (°C)	\dot{V}_f (L/min)	\dot{V}_p (L/min)
R1-50-20	49.93	43.23	19.85	24.75	1.04	0.99
R2-50-20	50.75	43.59	20.42	24.46	1.06	1.00
R3-50-20	49.58	43.02	19.57	24.92	1.03	1.00
R1-60-20	60.11	51.09	20.35	27.11	1.07	1.04
R2-60-20	59.69	50.13	20.49	27.02	1.06	1.06
R3-60-20	60.59	50.99	20.29	27.65	1.06	1.03

of the temperature polarization coefficient and results in a decrease of the partial vapour pressure difference. The reduction of partial vapour pressure difference is the reason for smaller mass flux as seen from Eq. (4). However, as can be seen from Eq. (19), the higher values of membrane thermal conductivity (using the parallel model for membrane thermal conductivity) leads to a higher total heat transfer coefficient, which is shown in Fig. 6. Thus, the heat transfer rate was larger in this case. From the comparison between experimental and theoretical results, the most appropriate model for the thermal conductivity of the membrane was acquired. It can be seen from Fig. 5, under the effect of ST4 spacer, that the deviation between theoretical and experimental mass flux was nearly 11% for the parallel model, while this difference was almost 5% and 3% for the two kinds of Maxwell model and series model, respectively. However, for the rate of heat transfer, the deviation was nearly 15% and 23% for the series and parallel model, respectively. For Maxwell’s model, the Type II model shown less difference than Type I with a deviation under 8% for both kinds of the Maxwell model. From the comparison, Maxwell Type II was the most appropriate model for estimating the thermal conductivity of the membrane.

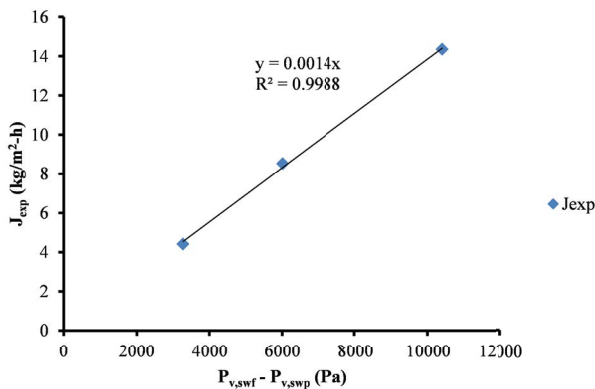


Fig. 4. Determination of water vapor permeability of the membrane.

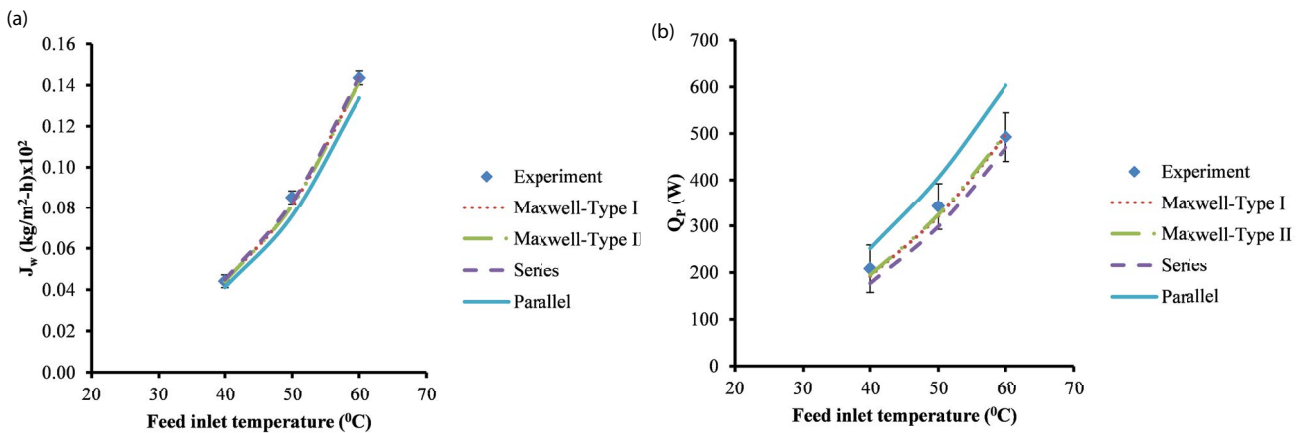


Fig. 5. Theoretical mass flux (a) and heat rate (b) of various models of membrane thermal conductivity under the effect of ST4 spacer.

4.3. Effect of membrane thermal conductivity model on the global heat transfer coefficient (U)

Based on the global heat transfer coefficient calculation in Eq. (19), it can be seen that when the thermal conductivity of the membrane was higher, the temperature deviation and the heat transfer resistance $\left(\frac{1}{k_m / \delta + J_w \Delta H_{v,w} / \Delta T_m}\right)$ were

smaller. Therefore, the total predicted heat transfer coefficient (U) became larger for the higher thermal conductivity value of the membrane (in this study, the differences of h_f and h_p between models are trivial, and these deviations can be neglected). It is shown in Fig. 6 that the total predicted heat transfer coefficient for the parallel model was the highest among the four models. This result led to the predicted heat rate in the parallel model being nearly 1.4 times higher than that in the remaining models.

4.4. Impact of membrane thermal conductivity model on temperature polarization coefficient

The partial vapour pressure difference between the membrane-feed and membrane-permeate side was caused by a temperature difference and allowed the water vapour to move across the membrane pores. The higher the thermal conductivity of the membrane was, the more significant the conduction heat loss. Therefore, using the model with a higher membrane thermal conductivity value introduced a reduction of the driving temperature difference and lowered the predicted mass flux of the DCMD module. It is shown in Fig. 7 that the temperature polarization coefficient for the parallel model was the lowest in comparison with the other models. This underestimation of TPC resulted in the lowest predicted mass flux for the parallel model, which was shown in Fig. 5a.

4.5. Effect of membrane thermal conductivity model on energy efficiency and GOR

There were two factors affecting thermal efficiency: membrane properties and operational parameters. The membrane characteristics were porosity, tortuosity, and

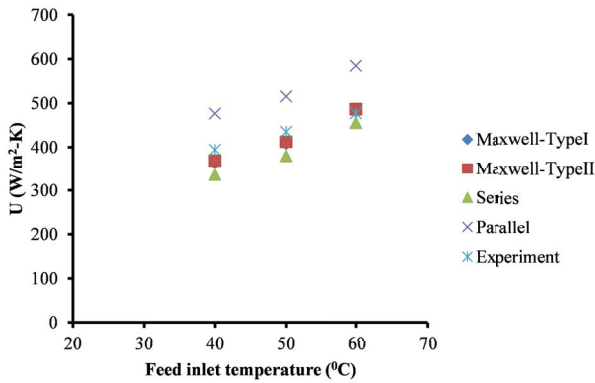


Fig. 6. Global predicted heat transfer coefficient for different membrane thermal conductivity models under the effect of ST4 spacer.

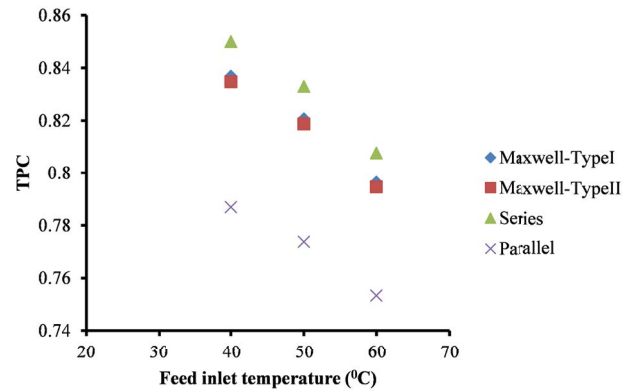


Fig. 7. Temperature polarisation coefficient for various thermal conductivity models of the membrane under the effect of ST4 spacer.

thermal conductivity. The operating parameters were the temperature and salinity at both sides of the DCMD module. In this study, only thermal conductivity of the membrane and temperature of the feed side were considered. As mentioned in Eq. (32), the energy efficiency was described as the latent heat of evaporation ($J_w \Delta H_{v,w}$) divided by the total heat transfer through the membrane (\dot{Q}_m). When the theoretical value of the membrane thermal conductivity was high, the temperature difference across the membrane was reduced which resulted in lower thermal efficiency because of lower mass flux. These explanations were coincident with the predicted results through various models in Fig. 8. The parallel model had the lowest values of energy efficiency through the investigated feed inlet temperature range.

For GOR, the maximum difference among the four models was only 8%. It can be clearly seen from Eq. (33), Fig. 5, and Fig. 9 that the lowest value of theoretical mass flux belonged to the parallel model because of its highest predicted membrane thermal conductivity. Also, the GOR calculation in all models depended only on the mass flux. Therefore, the lowest GOR value was for the parallel model. Consequently, the choice of thermal conductivity of the membrane should underestimate or overestimate the efficiency of using the input energy in the DCMD module to produce the permeate flux.

5. Conclusions

In this study, the effect of various membrane thermal conductivity models on theoretical mass flux, the heat transfer rate, the global heat transfer coefficient, TPC, energy efficiency, and GOR was investigated theoretically and experimentally. A mathematical model developed in MATLAB was used to estimate the temperatures at the membrane interface. The water vapour permeability of the hydrophobic membrane was also determined by theory and experiment, where the maximum difference was only 4.3% in the tested range of feed inlet temperature. It was concluded that Maxwell’s models, in particular, Maxwell Type II model gave the best agreement between the theoretical and experimental data in the case of mass flux and heat

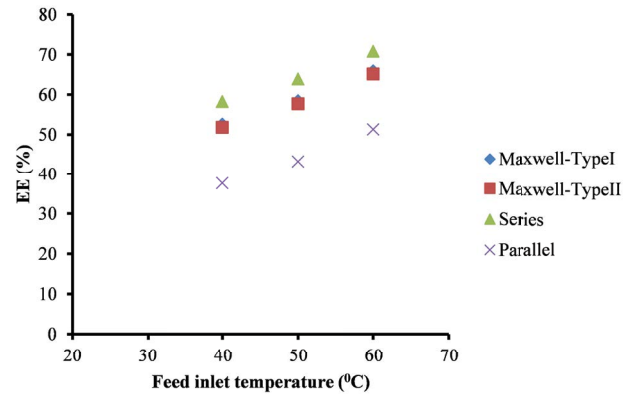


Fig. 8. Energy efficiency for different thermal conductivity models of the membrane.

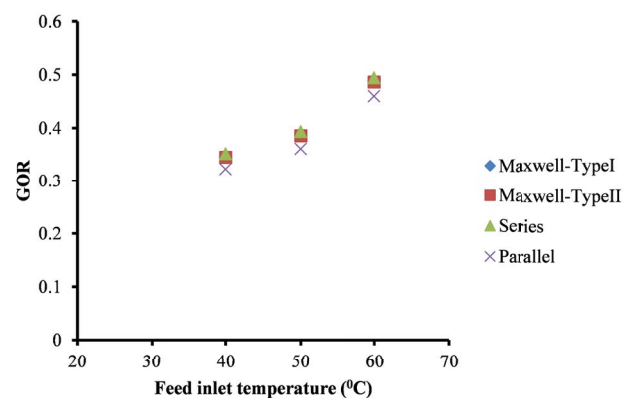


Fig. 9. The GOR for various models of membrane thermal conductivity.

transfer rate. On the contrary, the parallel model had the largest discrepancy for these two investigated factors. The parallel model with the highest value of membrane thermal conductivity acquired the lowest predicted mass flux, TPC and EE, whereas the predicted heat transfer rate and

the total heat transfer coefficient were the largest among the four proposed models. The GOR values for all models had small fluctuations with only 8% discrepancy.

In general, for thermal conductivity of the membrane, Maxwell Type II was recommended for further studies with extensive saline water, a wider range of flow rates and various kinds of spacers. The main contribution of this study is the proposed methodology for selecting the most appropriate model of membrane thermal conductivity which is based on experimental data of mass flux and heat transfer rate. This is very beneficial for the validation of numerical modelling for DCMD system.

Acknowledgment

This research was supported by the Australia Awards Scholarship and RMIT University. We thank Dr. Jason Velardo and two reviewers for comments that significantly improved the manuscript.

Symbols

A	—	Membrane area, m^2
C_m	—	Membrane distillation coefficient, $kg\ m^{-2}\ s^{-1}\ Pa^{-1}$
C_m^C	—	Membrane distillation coefficient for Knudsen-molecular diffusion mechanism, $kg\ m^{-2}\ s^{-1}\ Pa^{-1}$
C_m^D	—	Membrane distillation coefficient for molecular diffusion, $kg\ m^{-2}\ s^{-1}\ Pa^{-1}$
C_m^K	—	Membrane distillation coefficient for Knudsen mechanism, $kg\ m^{-2}\ s^{-1}\ Pa^{-1}$
$C_{p,f}$	—	Specific heat coefficient of water at the feed side, $J\ kg^{-1}\ K^{-1}$
$C_{p,p}$	—	Specific heat coefficient of water at permeate side, $J\ kg^{-1}\ K^{-1}$
DEV	—	Deviation between experimental and theoretical result, %
EE	—	Thermal efficiency, %
GOR	—	Gain output ratio
J_w	—	Experimental mass flux, $kg\ m^{-2}\ s^{-1}$
J_{wt}	—	Theoretical mass flux, $kg\ m^{-2}\ s^{-1}$
Kn	—	Knudsen number
L	—	Length of the flow channel, m
M	—	Molecular weight of water, $kg\ mol^{-1}$
Nu	—	Nusselt number
P_a	—	Entrapped air pressure, Pa
P_m	—	Mean pressure within the membrane pores (or total pressure), Pa
Pr	—	Prandtl number
\dot{Q}_c	—	Conduction heat loss through membrane matrix, W
\dot{Q}_f	—	Heat transfer rate through feed thermal boundary layer, W
\dot{Q}_F	—	Heat released by the feed, W
\dot{Q}_m	—	Heat transfer rate through the membrane, W
\dot{Q}_p	—	Heat transfer rate through permeate thermal boundary layer, W
\dot{Q}_p	—	Heat gained by the permeate, W
\dot{Q}_{pt}	—	Theoretical heat transfer rate, W
\dot{Q}_v	—	Latent heat transfer by vapour through membrane pores, W
R	—	Gas constant, $J\ mol^{-1}\ K^{-1}$

Re	—	Reynolds number
S	—	Feed salinity, $g\ kg^{-1}$
ST4	—	Stainless steel spacer
T_f	—	Bulk feed side temperature, K
$T_{f,in}$	—	Feed inlet temperature, K
$T_{f,out}$	—	Feed outlet temperature, K
T_m	—	Mean temperature at the membrane surface, K
$T_{m,f}$	—	Temperature at the feed-membrane interface, K
$T_{m,p}$	—	Temperature at the permeate-membrane interface, K
T_p	—	Bulk permeate side temperature, K
$T_{p,in}$	—	Permeate inlet temperature, K
$T_{p,out}$	—	Permeate outlet temperature, K
U	—	Global heat transfer coefficient of the DCMD process, $W\ m^{-2}\ K^{-1}$
\dot{V}	—	Volume flow rate, $L\ min^{-1}$
d_e	—	Collision diameter of water vapour, m
d_h	—	Hydraulic diameter, m
d_p	—	Membrane pore diameter, m
h_f	—	Heat transfer coefficient at feed side, $W\ m^{-2}\ K^{-1}$
h_m	—	Heat transfer coefficient of the whole membrane, $W\ m^{-2}\ K^{-1}$
h_p	—	Heat transfer coefficient at permeate side, $W\ m^{-2}\ K^{-1}$
k	—	Thermal conductivity of water, $W\ m^{-1}\ K^{-1}$
k_B	—	Boltzman constant, $J\ K^{-1}$
k_m	—	Thermal conductivity of membrane, $W\ m^{-1}\ K^{-1}$
l_m	—	Mesh size, m
\dot{m}_f	—	Mass flow rate at the feed side, $kg\ s^{-1}$
\dot{m}_p	—	Mass flow rate at permeate side, $kg\ s^{-1}$
$p_{v,swf}$	—	Partial pressure of water vapour at the feed-membrane surface, Pa
$p_{v,swp}$	—	Partial pressure of water vapour at the permeate-membrane surface, Pa
r	—	Mean pore size radius, m

Greek symbols

τ	—	Membrane tortuosity
ε	—	Membrane porosity
δ	—	Membrane thickness, m
λ_w	—	Mean free path, m
σ_w	—	Collision diameter of water vapour, m

Subscripts

f	—	Feed
p	—	Permeate

References

- [1] R.W. Schofield, A.G. Fane, C.J.D. Fell, Heat and mass transfer in membrane distillation, *J. Membr. Sci.*, 33 (1987) 299–313.
- [2] J. Phattaranawik, R. Jiraratananon, A.G. Fane, Heat transport and membrane distillation coefficients in direct contact membrane distillation, *J. Membr. Sci.*, 212 (2003) 177–193.
- [3] K.W. Lawson, D.R. Lloyd, Membrane distillation, *J. Membr. Sci.*, 124 (1997) 1–25.
- [4] M. Gryta, M. Tomaszewska, A.W. Morawski, Membrane distillation with laminar flow, *Sep. Purif. Technol.*, 11 (1997) 93–101.
- [5] M. Khayet, A. Velázquez, I. Mengual Juan, Modelling mass transport through a porous partition: effect of pore size distribution, *J. Non-Equilib. Thermodyn.*, 29 (2004) 279–299.

- [6] H.I. Plamenov, Model-Based Analysis and Optimization of Membrane Distillation, Faculty of Bioscience Engineering, Ghent University, 2017.
- [7] M.C. García-Payo, M.A. Izquierdo-Gil, Thermal resistance technique for measuring the thermal conductivity of thin microporous membranes, *J. Phys. D: Appl. Phys.*, 37 (2004) 3008–3016.
- [8] E.E. Gonzo, Estimating correlations for the effective thermal conductivity of granular materials, *Chem. Eng. J.*, 90 (2002) 299–302.
- [9] S. Al-Obaidani, E. Curcio, F. Macedonio, G. Di Profio, H. Al-Hinai, E. Drioli, Potential of membrane distillation in seawater desalination: thermal efficiency, sensitivity study and cost estimation, *J. Membr. Sci.*, 323 (2008) 85–98.
- [10] N. Loussif, J. Orfi, Comparative study of air gap, direct contact and sweeping gas membrane distillation configurations, *Membr. Water Treat.*, 7 (2016) 71–86.
- [11] J. Vanneste, J.A. Bush, K.L. Hickenbottom, C.A. Marks, D. Jassby, C.S. Turchi, T.Y. Cath, Novel thermal efficiency-based model for determination of thermal conductivity of membrane distillation membranes, *J. Membr. Sci.*, 548 (2018) 298–308.
- [12] R.W. Schofield, A.G. Fane, C.J.D. Fell, R. Macoun, Factors affecting flux in membrane distillation, *Desalination*, 77 (1990) 279–294.
- [13] J. Phattaranawik, R. Jiraratananon, A.G. Fane, C. Halim, Mass flux enhancement using spacer filled channels in direct contact membrane distillation, *J. Membr. Sci.*, 187 (2001) 193–201.
- [14] E. Curcio, E. Drioli, Membrane distillation and related operations: a review, *Sep. Purif. Rev.*, 34 (2005) 35–86.
- [15] P. Termpiyakul, R. Jiraratananon, S. Srisurichan, Heat and mass transfer characteristics of a direct contact membrane distillation process for desalination, *Desalination*, 177 (2005) 133–141.
- [16] S. Adnan, M. Hoang, H. Wang, Z. Xie, Commercial PTFE membranes for membrane distillation application: effect of microstructure and support material, *Desalination*, 284 (2012) 297–308.
- [17] Y.M. Manawi, M. Khraisheh, A.K. Fard, F. Benyahia, S. Adham, Effect of operational parameters on distillate flux in direct contact membrane distillation (DCMD): comparison between experimental and model predicted performance, *Desalination*, 336 (2014) 110–120.
- [18] A. Tamburini, M. Renda, A. Cipollina, G. Micale, M. Ciofalo, Investigation of heat transfer in spacer-filled channels by experiments and direct numerical simulations, *Int. J. Heat Mass Transfer*, 93 (2016) 1190–1205.
- [19] R. Ullah, M. Khraisheh, R.J. Esteves, J.T. McLeskey, M. AlGhouti, M. Gad-el-Hak, H. Vahedi Tafreshi, Energy efficiency of direct contact membrane distillation, *Desalination*, 433 (2018) 56–67.
- [20] H. Fan, Y. Peng, Application of PVDF membranes in desalination and comparison of the VMD and DCMD processes, *Chem. Eng. Sci.*, 79 (2012) 94–102.
- [21] M. Khayet, T. Matsuura, *Membrane Distillation: Principles and Applications*, Elsevier, Amsterdam, 2011.
- [22] Z. Li, Y. Peng, Y. Dong, H. Fan, P. Chen, L. Qiu, Q. Jiang, Effects of thermal efficiency in DCMD and the preparation of membranes with low thermal conductivity, *Appl. Surf. Sci.*, 317 (2014) 338–349.
- [23] J. Zhang, S. Gray, J.-D. Li, Predicting the influence of operating conditions on DCMD flux and thermal efficiency for incompressible and compressible membrane systems, *Desalination*, 323 (2013) 142–149.
- [24] G. Zuo, R. Wang, R. Field, A.G. Fane, Energy efficiency evaluation and economic analyses of direct contact membrane distillation system using Aspen Plus, *Desalination*, 283 (2011) 237–244.
- [25] H.C. Duong, L. Xia, Z. Ma, P. Cooper, W. Ela, L.D. Nghiem, Assessing the performance of solar thermal driven membrane distillation for seawater desalination by computer simulation, *J. Membr. Sci.*, 542 (2017) 133–142.
- [26] A. Criscuoli, M.C. Carnevale, E. Drioli, Evaluation of energy requirements in membrane distillation, *Chem. Eng. Process*, 47 (2018) 1098–1105.
- [27] Z. Kuang, R. Long, Z. Liu, W. Liu, Analysis of temperature and concentration polarizations for performance improvement in direct contact membrane distillation, *Int. J. Heat Mass Transfer*, 145 (2019) 118724.
- [28] M. Khayet, Solar desalination by membrane distillation: dispersion in energy consumption analysis and water production costs: a review, *Desalination*, 308 (2013) 89–101.
- [29] R. Long, X. Lai, Z. Liu, W. Liu, Direct contact membrane distillation system for waste heat recovery: modelling and multi-objective optimization, *Energy*, 148 (2018) 1060–1068.
- [30] S.T. Bouguecha, S.E. Aly, M.H. Al-Beirutty, M.M. Hamdi, A. Boubakri, Solar driven DCMD: performance evaluation and thermal energy efficiency, *Chem. Eng. Res. Des.*, 100 (2015) 331–340.
- [31] G. Guan, X. Yang, R. Wang, A.G. Fane, Evaluation of heat utilization in membrane distillation desalination system integrated with heat recovery, *Desalination*, 366 (2015) 80–93.
- [32] M. Khayet, M.P. Godino, J.I. Mengual, Modelling transport mechanism through a porous partition, *J. Non-Equilib. Thermodyn.*, 26 (2001) 1–14.
- [33] M. Qtaishat, T. Matsuura, B. Kruczek, M. Khayet, Heat and mass transfer analysis in direct contact membrane distillation, *Desalination*, 219 (2008) 272–292.
- [34] R.W. Schofield, A.G. Fane, C.J.D. Fell, Gas and vapour transport through microporous membranes: II. membrane distillation, *J. Membr. Sci.*, 53 (1990) 173–185.
- [35] R.W. Schofield, A.G. Fane, C.J.D. Fell, Gas and vapour transport through microporous membranes: I. Knudsen-poiseuille transition, *J. Membr. Sci.*, 53 (1990) 159–171.
- [36] A. Alkudhiri, N. Darwish, N. Hilal, Membrane distillation: a comprehensive review, *Desalination*, 287 (2012) 2–18.
- [37] K.G. Nayar, M.H. Sharqawy, L.D. Banchik, J.H. Lienhard V, Thermophysical properties of seawater: a review and new correlations that include pressure dependence, *Desalination*, 390 (2016) 1–24.
- [38] Q.L. Ve, K. Rahaoui, M. Bawahab, H. Faqeha, A. Date, A. Faghieh, A. Akbarzadeh, An experimental heat transfer investigation of using spacer in direct contact membrane distillation, *Energy Procedia*, 160 (2019) 223–230.
- [39] Q.L. Ve, K. Rahaoui, M. Bawahab, H. Faqeha, A. Date, A. Akbarzadeh, C.M. Do, L.Q. Nguyen, Experimental investigation of heat transfer correlation for direct contact membrane distillation, *J. Heat Transfer*, 142 (2019) 012001-1–012001-13.
- [40] I. Hitsov, L. Eykens, W.D. Schepper, K.D. Sitter, C. Dotremont, I. Nopens, Full-scale direct contact membrane distillation (DCMD) model including membrane compaction effects, *J. Membr. Sci.*, 524 (2017) 245–256.
- [41] M. Gryta, M. Tomaszewska, Heat transport in the membrane distillation process, *J. Membr. Sci.*, 144 (1998) 211–222.
- [42] K.W. Lawson, D.R. Lloyd, Membrane distillation: II. Direct contact MD, *J. Membr. Sci.*, 120 (1996) 123–133.
- [43] J. Zhang, S. Gray, J.-D. Li, Modelling heat and mass transfers in DCMD using compressible membranes, *J. Membr. Sci.*, 387–388 (2012) 7–16.
- [44] L. Martínez-Díez, M.I. Vázquez-González, F.J. Florido-Díaz, Study of membrane distillation using channel spacers, *J. Membr. Sci.*, 144 (1998) 45–56.
- [45] A.S. Jönsson, R. Wimmerstedt, A.C. Harrysson, Membrane distillation – a theoretical study of evaporation through microporous membranes, *Desalination*, 56 (1985) 237–249.
- [46] A.R. da Costa, *Fluid Flow and Mass Transfer in Spacer-Filled Channels for Ultrafiltration*, School of Chemical Engineering and Industrial Chemistry, University of New South Wales, Australia, 1993.
- [47] C.J. Geankoplis, *Transport Processes and Unit Operations*, Prentice-Hall International, Inc. 937, Englewood Cliffs, New Jersey 07632, USA, 1993.